Zero Thermal Expansion in a Nanostructured Inorganic-Organic Hybrid Crystal

Y. Zhang,[1,*] Z. Islam,[2] Y. Ren,[2] P. A. Parilla,[1] S. P. Ahrenkiel,[1] P. L. Lee,[2] A. Mascarenhas,[1] M. J. McNevin,[3] I. Naumov,[4] H.-X. Fu,[4] X.-Y. Huang,[5] and J. Li[5]

[1]*National Renewable Energy Laboratory, 1617 Cole Boulevard, Golden, Colorado 80401, USA*
[2]*Advanced Photon Source, Argonne National Laboratory, 9700 S. Cass Avenue, Argonne, Illinois 60439, USA*
[3]*Department of Chemistry and Biochemistry, University of Colorado, Boulder, Colorado 80309, USA*
[4]*Department of Physics, University of Arkansas, Fayetteville, Arkansas 72701, USA*
[5]*Department of Chemistry and Chemical Biology, Rutgers, The State University of New Jersey, Piscataway, New Jersey 08854, USA*

(Received 9 May 2007; published 19 November 2007)

There are very few materials that exhibit zero thermal expansion (ZTE), and of these even fewer are appropriate for electronic and optoelectronic applications. We find that a multifunctional crystalline hybrid inorganic-organic semiconductor, β-ZnTe(en)$_{0.5}$ (en denotes ethylenediamine), shows uniaxial ZTE in a very broad temperature range of 4–400 K, and concurrently possesses superior electronic and optical properties. The ZTE behavior is a result of compensation of contraction and expansion of different segments along the inorganic-organic stacking axis. This work suggests an alternative route to designing materials in a nanoscopic scale with ZTE or any desired positive or negative thermal expansion (PTE or NTE), which is supported by preliminary data for ZnTe(pda)$_{0.5}$ (pda denotes 1,3-propanediamine) with a larger molecule.

DOI: 10.1103/PhysRevLett.99.215901 PACS numbers: 65.40.De, 61.10.−i, 61.46.−w, 63.22.+m

The majority of the materials that are known to exhibit near zero thermal expansion (ZTE) in a broad temperature range are oxides and usually insulators, with a few nonoxide exceptions: e.g., YbGaGe being metallic [1], and some Prussian Blue analogues being ferromagnetic [2,3]. Traditional interests in ZTE materials have largely been in areas such as optics, heat-engine components, and kitchenwares. ZTE materials with applications in nonconventional areas such as electronics and optoelectronics are rare. Materials with ZTE may be found in three categories: (1) With isotropic ZTE, often achieved by alloying commonly available positive thermal expansion (PTE) and less available negative thermal expansion (NTE) materials. These materials are mostly oxides with open network structures [4–6], but they can also be ferromagnetic materials such as INVAR [4] and some members of the Prussian Blue family [2]. (2) With anisotropic thermal expansion (TE) but overall ZTE in volume, including lithium aluminum silicates [4] and the recently found metallic YbGaGe [1]. (3) With anisotropic TE and ZTE in one or two dimensions, but with nonzero TE in the other dimension(s) as well as in volume. The materials studied in this work belong to the last category. ZTE materials in category (2) are typically used in the form of polycrystalline aggregates, and so as the temperature changes, internal mesoscopic cracking is often a major concern [4]. When a ZTE material with mesoscopic domains is used as an active medium in electronics or optoelectronics, conductivity also suffers from the existence of grain boundaries. Therefore, if isotropic ZTE is not available, uniaxial or biaxial ZTE is preferred and is adequate for numerous applications, such as solid state laser cavities, semiconductor lasers, and x-ray monochromators and metrologies. A TE coefficient in the range of $|\alpha| < 2 \times 10^{-6}$ K^{-1} is generally considered as "very low TE" [4]. While the Prussian Blue analogue shows small isotropic TE with an average $\alpha \sim -1.5 \times 10^{-6}$ K^{-1} between 4 and 300 K [2], the hybrid crystal studied here offers uniaxial but significantly smaller TE with $|\alpha| < 4.3 \times 10^{-7}$ K^{-1} in a broader temperature range of 4–400 K. More significantly, the hybrid approach offers a new route to designing materials with any desired TE.

Hybrid nanocomposites have lately received a great deal of interest in both fundamental science and applications [7,8]. The materials, $MQ(L)_x$ (MQ for II–VI semiconductor, L for organic molecule), to be investigated here belong to a new family of multifunctional hybrid crystals that consist of subnanometer inorganic building blocks interconnected or coordinated by small organic molecules [9,10]. They can be classified into three groups: 3-D, 2-D, and 1-D structures, depending on the bonding situation between the inorganic and organic components. Here we focus on the 3-D structures, which are inorganic-organic superlattices with a well-defined stacking axis. It is along this axis that the unusual TE is found. The structures have been shown to be fully ordered structures without the physical and chemical fluctuations typically found in other hybrid materials and nanostructures [9–11]; they have also been shown, both experimentally and theoretically, to possess unique electronic and optical properties [9,10,12–14] that are highly desirable for applications in optoelectronics, including a massive band gap blueshift (~1.4 eV) from that of the inorganic semiconductor [10,13], and exceedingly strong band-edge excitonic absorption (up to ~10^6 cm^{-1}) [13,14]. Together with low-weight and the flexibility of the organic material, these properties make them very promising candidates as active

materials for making high efficiency semiconductor lasers, ultrathin and flexible solar cells, and light-emitting and detecting devices. Additionally, it is possible to dope them for use as transparent conducting materials [14]. While chemical and thermal stability are two major problems for most hybrids in applications, the hybrid nanostructures investigated in this work are found to be exceptionally stable in the air, even under the illumination of a UV laser. Not only do the crystal structures remain unchanged, but also their electronic and optical properties after a few years of air exposure or upon heating to >200 °C, a feature attributed to the strong covalent bonding throughout the structure.

The 3-D hybrid superlattices $MQ(L)_{0.5}$ [M = Zn or Cd; $Q = S$, Se, or Te; and L = en (ethylenediamine or 1,2-ethanediamine, $C_2H_8N_2$) or pda (1,3-propanediamine, $C_3H_{10}N_2$)] are composed of two-monolayer slabs of II–VI semiconductors that are interconnected by the organic molecules [9–11]. They crystallize in orthorhombic crystal systems. For instance, α-$MQ(\text{en})_{0.5}$ and $MQ(\text{pda})_{0.5}$ are derived from the wurtzite structure and belong to the space group $Pbca$ and $Cmc2_1$, respectively; β-$MQ(\text{en})_{0.5}$ is derived from the zinc-blende (ZB) structure and belongs to the space group $Pnnm$. Figure 1 shows the crystal structure of a prototype hybrid superlattice, β-ZnTe(en)$_{0.5}$. The general plan for obtaining ZTE or NTE in a broad temperature range has been to have a crystal structure with transverse vibrations that reduce the distance between nonbonded atoms, which balances or overbalances the usual PTE [15,16]. In practice, the search for ZTE materials has focused primarily on an open structure with a relatively rigid framework made up of strongly bonded small polyhedra [2,4,16,17]. The hybrid structure shown in Fig. 1 obviously falls out of this practical guideline.

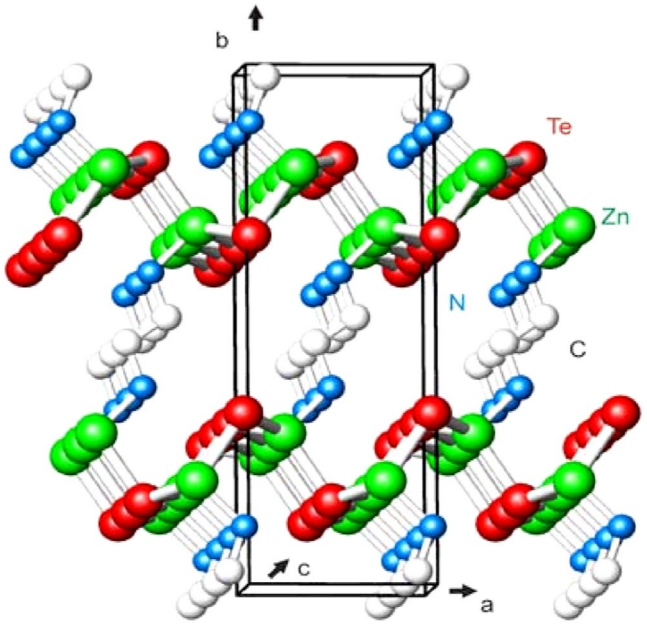

FIG. 1 (color online). The crystal structure of β-ZnTe(en)$_{0.5}$, determined by single-crystal x-ray diffraction. Two-monolayer-thick ($\bar{1}10$) ZnTe slabs are interconnected by ethylenediamine molecules bonded to Zn atoms. Hydrogen atoms are omitted for clarity. The unit cell, as outlined, contains a pair of ZnTe slabs, rotated 180° with respect to each other about the b axis.

In this work, the TE of β-ZnTe(en)$_{0.5}$, in both single-crystal and powder form, has been carefully investigated; ZnTe(pda)$_{0.5}$ has also been briefly examined. β-ZnTe(en)$_{0.5}$ powder samples were measured between 4.2 and 400 K using 115.562 keV ($\lambda = 0.10726$ Å) x rays and a MAR345 image plate available on the 11-ID-C beam line at the Advanced Photo Source (APS) at Argonne National Laboratory. The structure is solved at each temperature by Rietveld refinements using the GSAS program with an accuracy $\delta d/d \sim 4 \times 10^{-4}$. High-resolution, single-crystal x-ray diffraction studies were performed from 12 to 330 K on the 1-BM-C beam line at the APS, with an accuracy $\delta d/d \sim 10^{-4}$ [18]. X-ray photons of 20.0161 keV ($\lambda = 0.619\,423$ Å) were selected using a Si(111) monochromator and were focused down to a spot size of approximately 0.3 mm × 0.5 mm on single-crystal samples with dimensions of $\sim 1 \times 1 \times 0.02$ mm. $(0, k, 0)$ diffractions with $k = 2n$ and n = 1–10 were used to determine the b lattice constant. The single-crystal sample was also measured by a Siemens SMART diffractometer (Mo Ka, $\lambda = 0.710\,73$ Å) with a CCD area detector and graphite monochromator at the University of Colorado at Boulder from 140 to 300 K. The lattice parameters were determined by general refinement. Full unit-cell refinements were performed at 140 and 300 K. A single-crystal sample of ZnTe(pda)$_{0.5}$ was also examined using the Siemens machine with general refinements performed at a few temperature points, mainly to test how substituting the organic molecule might affect the TE in the superlattice stacking direction. The lattice parameters are, for β-ZnTe(en)$_{0.5}$, at 4.2 and 300 K, respectively, a = 5.6**569**(2) and 5.6**787**(2) Å, b = 17.19**83**(5) and 17.19**98**(6) Å (stacking axis), c = 4.3**429**(1) and 4.3**523**(1) Å, from powder diffraction; for ZnTe(pda)$_{0.5}$, at 134 and 300 K, respectively, a = 20.2**194**(104) and 20.2**082**(53) Å (stacking axis), b = 7.0**470**(23) and 7.0**671**(18) Å, c = 6.**8773**(36) and 6.**9002**(18) Å, from single-crystal diffraction. (The use of boldface numbers is to show more clearly the digital places for the changes between two temperatures.)

Figure 2 shows the temperature dependence of the lattice constants for β-ZnTe(en)$_{0.5}$. The TE increases in the order of b, c, and a. From 4.2 K to 300 K, $|\delta b|/b$ is found to be less than 1.5×10^{-4}, which is more than an order of magnitude smaller than $\delta c/c \approx 2.2 \times 10^{-3}$. The latter is very close to the TE of 2.5×10^{-3} for ZnTe [19], which is understandable because the c axis is the least distorted axis of ZnTe. Without distortion, c would be the [110] lattice

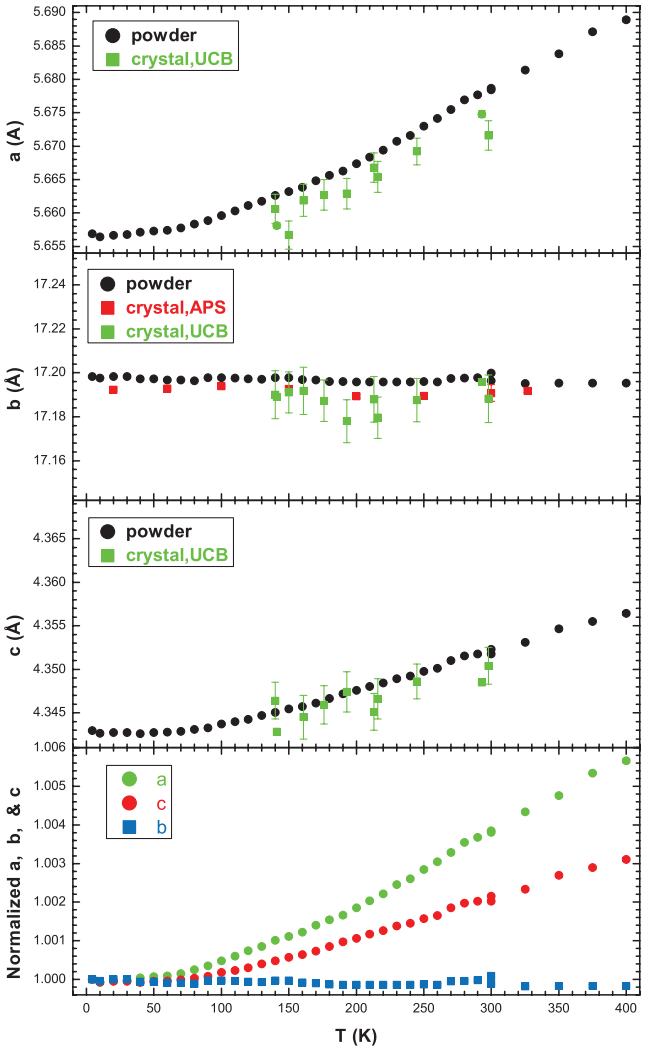

FIG. 2 (color). The temperature dependence of the lattice constants, a, b, and c for β-ZnTe(en)$_{0.5}$, measured on both powder and single-crystal samples and on different x-ray diffraction systems. The span of the vertical axis in the three upper panels is ~0.654% of the respective lattice constant.

spacing of the ZB structure, $a_{ZB}/\sqrt{2} = 4.313$ Å (1.6 K, a_{ZB} is the lattice constant of ZnTe), compared to the actual value of 4.343 Å (4.2 K). However, $\delta a/a \approx 3.8 \times 10^{-3}$ is found to be significantly larger than that of ZnTe. This axis, corresponding to the ZB [001] axis, is strongly distorted with $a = 5.657$ Å (4.2 K) compared to $a_{ZB} = 6.10$ Å (1.6 K). One may intuitively divide the b axis into three segments, $L_{\text{Te-Te}}$ (roughly the thickness of the inorganic slab), $L_{\text{N-N}}$ (the length of the organic molecule), and $L_{\text{Te-N}}$ (the connection of the two components), with $b = 2(L_{\text{Te-Te}} + L_{\text{N-N}} + 2L_{\text{Te-N}})$, and then examine the TE of each segment. Both powder and single-crystal refinement data (below 300 K) have indicated that TE is positive for $L_{\text{Te-Te}}$ and $L_{\text{Te-N}}$, but negative for $L_{\text{N-N}}$, which offers direct insight into the unusually small TE, i.e., a delicate balance between the PTE and NTE of different segments on a unit-cell scale. For instance, between 4 and 300 K, $L_{\text{Te-Te}} =$ 2.709(3) and 2.719(4) Å, $L_{\text{Te-N}} = 0.966(18)$ and 1.124(21) Å, $L_{\text{N-N}} = 3.958(33)$ and 3.632(39) Å, from the powder refinement data.

It is a formidable task to account quantitatively for the TE in a complex anisotropic system [20]. We attempt to identify only a few vibrational modes that could contribute to NTE and thus balance the readily available PTE mechanisms, under the widely used geometrical consideration of the lattice vibration [15,16,20,21]. A linear response theory, implemented in the density-function code ABINIT [22], has been applied to calculate the phonon spectrum of β-ZnTe(en)$_{0.5}$, using the experimental lattice parameters. An 80 Ry energy cutoff is used in the plane-wave expansion. The Brillouin-zone integration is performed using the special k-points scheme with a mesh of $4 \times 2 \times 4$. There are indeed a number of transverse and transverse-longitudinal (mixed) modes that can be excited in the experimental temperature range. For example, shown in Fig. 3 are the four lowest-frequency optical modes at the Γ point (~14–53 cm^{-1}). Modes no. 4, no. 6, and no. 7 represent the transverse vibrations of the inorganic slabs (dragging the organic molecules along with them) along the c axis that is perpendicular to the relatively strong bonds within the a-b plane. Mode no. 5 is a libration mode [20] about the b axis. These modes are likely among those contributing to the NTE of the organic segment, particularly in the relatively low-temperature region. Their frequencies are in a similar frequency region in which transverse modes are found to contribute to NTE in other materials [23,24]. A typical behavior of transverse modes, the frequency blueshift with increasing temperature [23,24], has actually been observed in the Raman

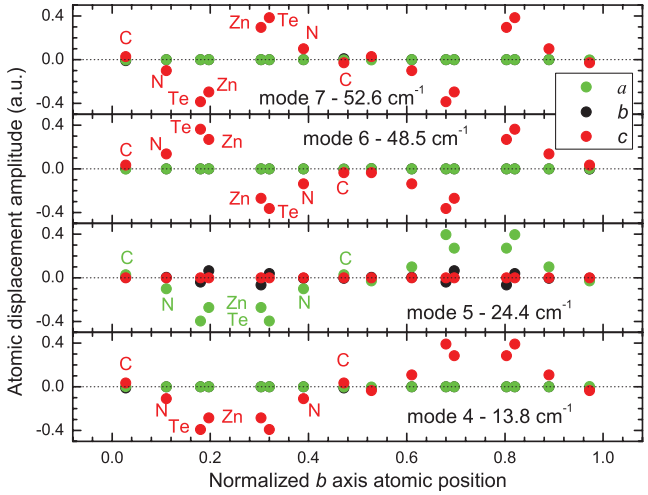

FIG. 3 (color). Atomic vibration amplitudes with respect to average crystallographic sites, along the three principle axes a, b, and c of β-ZnTe(en)$_{0.5}$, for atoms within the unit cell (H atoms are not shown for clarity) defined by their b coordinates. Included are the four lowest optical phonon modes at the Γ point.

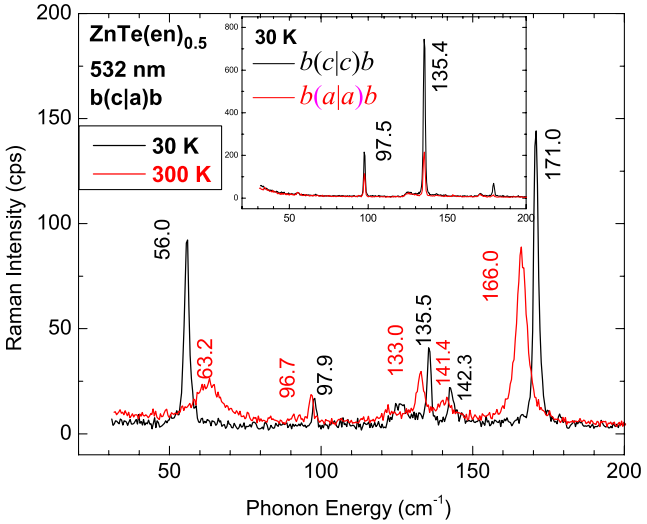

FIG. 4 (color online). Raman spectra of β-ZnTe(en)$_{0.5}$ measured at 30 and 300 K with cross polarization $(c|a)$. The inset shows the 30 K spectra with parallel polarization $(a|a)$ and $(b|b)$. The equivalent slit width was 0.5 cm^{-1}.

study for this crystal. Figure 4 shows the polarized first-order Raman spectra at 30 and 300 K, measured at near backscattering geometry, using a system composed of a SPEX1403 double-grating spectrometer, C31034 GaAs PMT, and a 30 mW 532 nm laser. The low-temperature Raman lines are sharp (e.g., the linewidth of the 135.4 cm^{-1} mode is only 0.8 cm^{-1} measured at 0.2 cm^{-1} resolution), reflecting the high crystalline quality of the sample, consistent with a very small mosaic spread of $\sim$0.01 degrees observed for the $(0, k, 0)$ Bragg peaks. A particularly interesting Raman line is the one at 56.0 cm^{-1} (30 K), which shows a large *blueshift* to 63.2 cm^{-1}, or a 12.9% increase, when reaching 300 K. This Raman line is tentatively assigned to mode no. 7 calculated to be 52.6 cm^{-1}. Although most of the other Raman lines exhibit the normal temperature dependence, i.e., redshifting with increasing temperature, we note that some of them show rather weak temperature dependence, e.g., 142.3 cm^{-1} $\rightarrow$ 141.4 cm^{-1} (-0.6%) compared to the strongest line in this spectral region that shows a much larger but typical redshift, 135.4 cm^{-1} $\rightarrow$ 133.0 cm^{-1} (-1.8%). A small frequency shift usually means a small Grüneisen parameter and thus a small contribution to TE. There is indeed a calculated mode at 139.5 cm^{-1} (mode no. 19).

The structural diversity within the $MQ(L)_{0.5}$ group, including the selection of the phase, and the freedom in changing either the inorganic component or the organic molecule, should offer room to further fine-tune the TE. Preliminary data on ZnTe(pda)$_{0.5}$ seem to suggest that the structure with a longer molecule has a somewhat larger and negative TE ($\sim -6 \times 10^{-4}$ from 134 to 300 K). Hybrid crystals of the 3-D structure have been synthesized with L containing up to 8 carbon atoms [25], and of the 2-D structure with thicker inorganic slabs [26], which should provide greater flexibility for engineering the TE. Additionally, the 1-D hybrid structure [10] and 3-D quantum dot arrays interconnected by organic molecules [27] might offer opportunities to extend the same design principle for achieving ZTE in higher dimensionalities.

The work performed at NREL was supported by NREL LDRD and U. S. DOE/OS/BES, under Contract No. DE-AC36-99GO10337; at ANL/APS, under Contract No. DE-AC02-06CH11357; at Arkansas, by Army congressional support and Oklamoma-Arkansas MRSEC; and at Rutgers, by NSF (No. DMR-0422932).

*yong_zhang@nrel.gov

[1] J. R. Salvador, F. Gu, and T. Hogan *et al.*, Nature (London) **425**, 702 (2003).
[2] S. Margadonna, K. Prassides, and A. N. Fitch, J. Am. Chem. Soc. **126**, 15390 (2004).
[3] K. W. Chapman, P. J. Chupas, and C. J. Kepert, J. Am. Chem. Soc. **128**, 7009 (2006).
[4] R. Roy, D. K. Agrawal, and H. A. McKinstry, Annu. Rev. Mater. Sci. **19**, 59 (1989).
[5] T. A. Mary *et al.*, Science **272**, 90 (1996).
[6] A. W. Sleight, Annu. Rev. Mater. Sci. **28**, 29 (1998).
[7] D. B. Mitzi, in *Progress in Inorganic Chemistry*, edited by K. Karlin (John Wiley & Sons, Inc., New York, 1999), p. 1.
[8] C. Sanchez *et al.*, J. Mater. Chem. **15**, 3559 (2005).
[9] X. Y. Huang, J. Li, and H. X. Fu, J. Am. Chem. Soc. **122**, 8789 (2000).
[10] X. Y. Huang *et al.*, J. Am. Chem. Soc. **125**, 7049 (2003).
[11] Z. X. Deng, L. B. Li, and Y. D. Li, Inorg. Chem. **42**, 2331 (2003).
[12] H. X. Fu and J. Li, J. Chem. Phys. **120**, 6721 (2004).
[13] B. Fluegel *et al.*, Phys. Rev. B **70**, 205308 (2004).
[14] Y. Zhang *et al.*, Phys. Rev. Lett. **96**, 026405 (2006).
[15] A. Sleight, Nature (London) **425**, 674 (2003).
[16] J. S. O. Evans, J. Chem. Soc. Dalton Trans. **1999**, 3317 (1999).
[17] A. L. Goodwin, K. W. Chapman, and C. J. Kepert, J. Am. Chem. Soc. **127**, 17980 (2005).
[18] J. C. Lang *et al.*, Rev. Sci. Instrum. **70**, 4457 (1999).
[19] O. Madelung, *Semiconductors—Basic Data* (Springer, Berlin, 1996).
[20] G. D. Barrera *et al.*, J. Phys. Condens. Matter **17**, R217 (2005).
[21] T. H. K. Barron, Ann. Phys. (N.Y.) **1**, 77 (1957).
[22] X. Gonze *et al.*, Comput. Mater. Sci. **25**, 478 (2002).
[23] J. N. Hancock *et al.*, Phys. Rev. Lett. **93**, 225501 (2004).
[24] K. W. Chapman *et al.*, Physica (Amsterdam) **385B**, 60 (2006).
[25] X. Y. Huang and J. Li (unpublished).
[26] X. Y. Huang and J. Li, J. Am. Chem. Soc. **129**, 3157 (2007).
[27] J. E. Murphy *et al.*, J. Am. Chem. Soc. **128**, 3241 (2006).